3D Eddy Current and Temperature Field Analysis of Large Hydro-generators in Leading Phase Operations

Ning Wang, Huifang Wang, and Shiyou Yang

***Abstract*—As a common practice, a large hydro-generator will operate in leading phase conditions to absorb the reactive power of the power grid. However, the accurate and precise prediction of the leading phase operation capacity of a large hydro-generator has always been a formidable challenge to engineers and academicians because it is extremely hard to compute the eddy currents and losses as well as the local overheating in the pressure plate and finger. To address this problem, a full three dimensional (3D) finite element model and method of the coupled eddy current and temperature fields in the end region of a large hydro-generator are developed. The equivalent medium parameters used in the computations are comprehensively discussed. Moreover, some numerically based solution methodologies for accurate computation of the field and armature currents under different leading phase conditions are proposed. Numerical results on the coupled eddy current and temperature fields in the end regions of a 250 MW hydro-generator confirm positively the feasibility of the present work.**

***Index Terms*—Eddy current field, hydro-generator, 3D finite element method, temperature field.**

I. Introduction

GENERALLY, a large hydro-generator is required to work in leading phase conditions to absorb the reactive power of the power grid under some abnormal cases. As it is well known, the local overheating in the end region is one critical factor to restrict the leading phase operation capacity of a generator. However, the precise determination of the temperature fields has always been formidable challenges to both engineers and academicians because of the complicated nature of the coupled eddy current-temperature fields in senses of a complicated 3D geometry and the nonlinear behavior of the ferromagnetic materials [1]-[2].

To solve the electromagnetic and temperature field distributions in the end region of a large generator including a hydro-generator, new models and methods are continuously being developed and applied [3]-[7]. In [3], the quasi-3D finite element method is applied to investigate the eddy current field in the end region of a 1000 MW turbo-generator; In [4], the temperature field in the stator windings end of large synchronous generators is numerically studied; In [5] and [6], the electromagnetic fields in the end region of a large turbo-generator are computed; and in [7], the influence of the metal screen materials on the 3D electromagnetic field and eddy current loss in the end region of a turbo-generator are studied. Nonetheless, the coupled eddy current and temperature fields in the end region of large hydro-generators in leading phase operations have not been comprehensively studied in literatures.

To comprehensively understanding the characteristics of the coupled eddy and temperature fields in the end region of large hydro-generators, the full 3D finite element models and methods are proposed and implemented on a 250 MW hydro-generator to investigate its eddy current field and temperature field distributions under leading phase operation conditions. Also, the equivalent medium parameters used in the computations are comprehensively discussed. Moreover, some numerically based solution methodologies for accurate computations of the field and armature currents under different working conditions are proposed.

Manuscript was submitted for review on 29, April, 2018.

Wang Ning, Wang Huifang and Yang Shiyou are with the College of Electrical Engineering, Zhejiang University, Hangzhou 310027, China(email:wangningzju@163.com,huifangwang@zju.edu.cn;eesyyang@zju.edu.cn)

Digital Object Identifier 10.30941/CESTEMS.2019.00028

II. Finite Element Model of the Coupled Eddy Current and Temperature Field

To compute the coupled eddy current and losses as well as the temperature fields in the end region, especially the pressure plate and finger, of a hydro-generator, a full 3D finite element method is used.

A. Eddy Current Field

Since the armature winding in a hydro-generator is generally a fractional slot one, a unit motor, a minimal part of the end region of a hydro-generator [8]-[10], as shown in Fig.1, is modeled in this study.

To precisely simulate the complicated 3D geometry of the end regions of a large hydro-generator and the saturation of the ferromagnetic materials, the full 3D harmonic finite element model and method based on the vector magnetic potential A and the scalar electric potential φ are developed. Generally, the materials in the end region of a hydro-generator include winding conductors, ferromagnetic materials, and air; and these materials correspond, respectively, to the regions V_1, V_2 and V_3 of Fig. 2. The governing equations in these regions are

$$\begin{cases} \nabla\times\left(\nu\nabla\times\boldsymbol{A}\right)-\nabla\left(\nu\nabla\bullet\boldsymbol{A}\right)+j\omega\sigma\boldsymbol{A}+\sigma\nabla\varphi=\boldsymbol{J}_s \\ \nabla\bullet\left(-j\omega\sigma\boldsymbol{A}-\sigma\nabla\varphi\right)=0 \end{cases} \text{ in } V \quad (1)$$

$$\nabla\times\left(\nu\nabla\times\boldsymbol{A}\right)-\nabla\left(\nu\nabla\bullet\boldsymbol{A}\right)=0 \quad \text{in } V_2 \tag{2}$$

$$\nabla\times\left(\nu_0\nabla\times\boldsymbol{A}\right)-\nabla\left(\nu_0\nabla\bullet\boldsymbol{A}\right)=0 \quad \text{in } V_3 \tag{3}$$

where, σ and ν are, respectively, the conductivity and reluctivity of the conductor; ν_0 is the reluctivity of the air; $\boldsymbol{J}_s$ is the source current density.

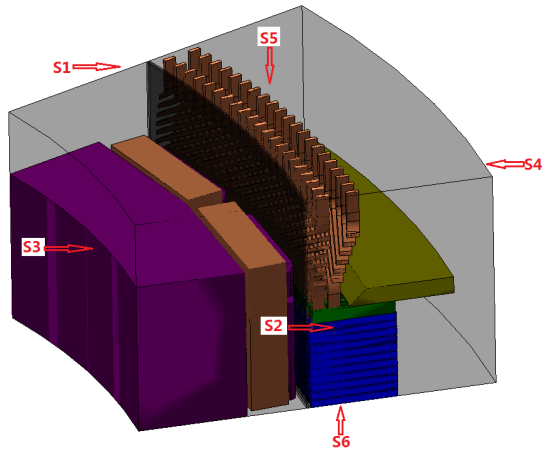

Fig. 1. The solid model of a hydro-generator.

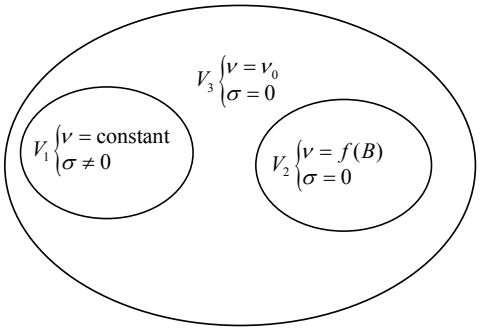

Fig. 2. The schematic diagram of an eddy current field problem.

The boundary conditions of the eddy current field for the exterior surfaces include the flux parallel boundary condition on surfaces S_3, S_4, S_5, and S_6; the periodical boundary condition on surfaces S_1 and S_2, as depicted in Fig. 1. Moreover, the periodical boundary condition on surfaces S_1 and S_2 is given as

$$\mathbf{A}\Big|_{s_1}=-\mathbf{A}\Big|_{S_2} \quad \text{(for an odd } d\text{)} \tag{4}$$

$$\mathbf{A}\Big|_{s_1}=\mathbf{A}\Big|_{S_2} \quad \text{(for an even } d\text{)} \tag{5}$$

where $q=m+c/d$ is the number of slots per phase per pole.

From the solid model of Fig. 1, it is obvious that the end region of a large hydro-generator is overwhelmingly complex in both geometry and material distribution. Consequently, it is formidable to model every detail in the full 3D coupled eddy current and temperature fields. In this regard, the laminated core is modeled using a bulk one to compromise the requirements on solution accuracy and speed in the finite element analysis. To start with, an equivalent magnetization curve of the ferromagnetic material used in the core is determined by using a Homogenization method based on a magnetostatic field analysis from

$$\hat{\mu}_i=\frac{\hat{\boldsymbol{B}}_i}{\hat{\boldsymbol{H}}_i} \tag{6}$$

$$\hat{\boldsymbol{B}}_i=\sum_{j=1}^{N}\Delta\boldsymbol{V}_j\boldsymbol{B}_j\Big/\sum_{j=1}^{N}\Delta\boldsymbol{V}_j \tag{7}$$

$$\hat{\boldsymbol{H}}_i=\sum_{j=1}^{N}\Delta\boldsymbol{V}_j\boldsymbol{H}_j\Big/\sum_{j=1}^{N}\Delta\boldsymbol{V}_j \tag{8}$$

where B_j and H_j are, respectively, the magnetic flux density and the magnetic field intensity of element j in the laminated iron core; ΔV_j is the volume of element j in the laminated iron core.

Moreover, to further increase the solution speed without any compromise on the solution accuracy, the stator multi-turns winding is modeled by using a bulk conductor. Consequently, a virtual conductivity is proposed to suppress the corresponding skin effect caused by this simplification.

Once the eddy current fields are determined using the full 3D finite element analysis, the heat generation in the iron and the conductor are determined, respectively, from:

$$P=\sum_i k\,p_a B^2 f^{1.3}\Delta G_i\,, \tag{9}$$

where, k is a coefficient (1.3 for the core and 1.7 for the tooth), ΔG_i is the weight of the i^{th} element in the iron material, f is the frequency, and

$$P=\sum_i \sigma J^2\Delta V_i \tag{10}$$

where, σ is the conductivity of the conductor, ΔV_i is the volume of the i^{th} element in the conductor.

B. *Temperature Field*

In the thermal analysis of the 3D finite element simulations, the air regions are excluded from the numerical model to reduce the computational burdens. Consequently, one uses an equivalent convection coefficient in the interface of the air and other medium to model the heat diffusion. Moreover, the averaged heat generation in one period in the harmonic eddy current field solutions is used in the temperature field analysis, and the governing equation for the full 3D steady-state temperature fields is

$$\frac{\partial}{\partial x}(\mu_x\frac{\partial T}{\partial x})+\frac{\partial}{\partial y}(\mu_y\frac{\partial T}{\partial y})+\frac{\partial}{\partial z}(\mu_z\frac{\partial T}{\partial z})=-q \tag{11}$$

$$-\lambda\frac{\partial T}{\partial n}\Big|_S=\alpha\left(T-T_f\right) \tag{12}$$

where; T is the temperature; μ_x, μ_y, and μ_z are, respectively, the thermal conductivity in x, y, z directions; q is the heat density; λ is the thermal conductivity; α is the convection coefficient.

The equivalent convection coefficients between the interfaces of the air and other medium, as shown in Fig. 3, are derived in the following paragraphs.

In a_1, the convection coefficient α is zero; In a_2, a_3, a_4, the convection coefficients are the same as that in surface B. In a_5, $\alpha=(\boldsymbol{N}_u\lambda)/\boldsymbol{D}$ (approximately equal to that in A, N_u=8.235, λ is the heat dissipation coefficient of air , and D is the distance between the pressure plate and the end cover); In a_6, a_7, a_8, the convection coefficients are the same as that in interface D; In a_9, the convection coefficients are the same as that in the interface C.

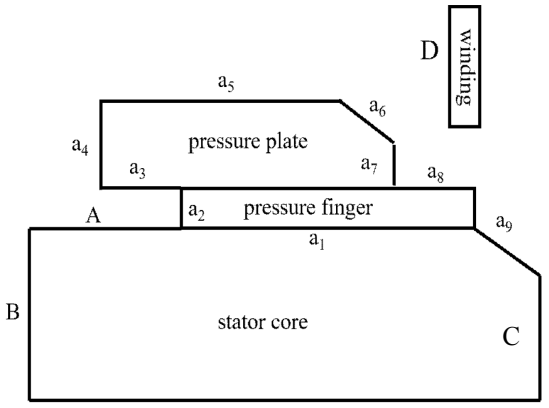

Fig.3. The schematic diagram of the interface between air and other medium.

Moreover, the convection coefficient in interface *A* is

$$\alpha = \frac{1+0.25V_{d1}}{0.045} \tag{13}$$

$$V_{d1} = 0.8V_d \ , \ V_d = 0.2U_2 \tag{14}$$

where, U_2 is the tangential speed of the air gap,

$$U_2 = \frac{2\pi Rf}{p} = 74.5 \tag{15}$$

where, R is air gap radius, f=50 Hz, p is the number of pole pairs.

The heat convection coefficient in interface *B* is generally given to be 40. The convection coefficient in interface *C* is

$$\alpha = 28(1+\sqrt{U_\delta}) \tag{16}$$

where, U_δ is the average wind speed at the air gap, and $U_\delta = U_2/2$.

The convection coefficient in interface *D* is

$$\alpha = \frac{(1+0.07U_2)\times 10^4}{C_s} \tag{17}$$

where, C_s is determined using Fig.4.

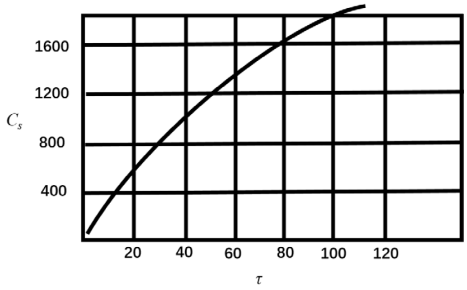

Fig.4. The relationship between C_s and pole pitch τ

III. Determination of the Field and Armature Currents

In a harmonic FEM analysis, one needs to determine the amplitude and the phase of the armature current, as defined in (18):

$$i = \sqrt{2}I\cos(\omega t + \lambda) \tag{18}$$

where, i is the armature current; I, and λ are , respectively, the amplitude and the phase of the armature current; ω is the angular frequency of the current.

However, the determination of the exact values for the amplitudes and phases of both field and armature coils is not an easy task. To address this issue, a solution methodology is proposed in this paper.

A. Initial Phase of Armature Current.

According to the basic theory of electrical machinery, as depicted in Fig. 5, the magnetic field B_0 of the exciting (field) coil will lead $\Psi_0+\pi/2$, as given in 19, electrical degree of the magnetic field B_a of the armature reaction field. Also, when the current of Phase *A* reaches its maximum value, the geometry axis of Phase *A* coil coincides with the axis of B_a. Based on these observations, the axis of the excitation coil will lead $\Psi_0+\pi/2$ electrical degree of the axis of phase A phase coil. Moreover, Ψ_0 is given by

$$\Psi_0 \approx \arctan\frac{U^*\sin\varphi + I_a^* X_q^*}{U^*\cos\varphi} \tag{19}$$

where X_q is the quadrature axis reaction reactance of the generator. U^* is 1 in the case study since the generator is connected to a definite power grid. All variables used in (19) are related value and dimensionless.

In practical application, the axis of the excitation magnetic coil does not exactly lead $\Psi_0+\pi/2$ but θ_1 electrical degree of the axis of Phase *A* coil. Consequently, the initial phase λ of phase *A* coil current is approximated as

$$\lambda = \theta_1 - (\frac{\pi}{2} + \Psi_0) \tag{20}$$

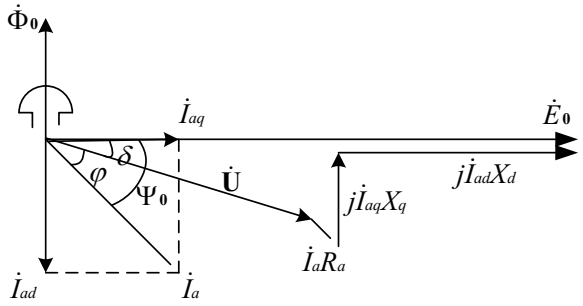

Fig.5. The phasor diagram of a salient-pole synchronous generator

B. Initial Amplitude of the Armature Current I_a (Phase A)

One assumes that the output power P_o of the generator remains constant in different operating conditions, i.e.,

$$P_o = mUI_a\cos\varphi = const \tag{21}$$

where *m* is the number of phases, *U* is the terminal voltage of the grid, cosφ is the power factor.

As *m* and *U* are fixed, (21) is modified as:

$$I_a\cos\varphi = const \tag{22}$$

Since I_a and cosφ in the rated operating condition are given, one can determine approximately the corresponding I_a in the leading phase operating condition if the leading phase depth cosφ is given.

C. The Exact Phase of the Armature Current

Due to the errors in the parameters used in 19 and the errors of the exact axis position of phase A coil arising from the fractional slot characteristics, the result given by 20 and 21 is only an approximated one. Hence, a finer adjustment of the

approximated results are implemented by repeatedly adjusting λ in the numerical computation of electromagnetic fields until the excitation magnetic field B_0 leads $\Psi_0+\pi/2$ electrical degree of the magnetic field of the armature reaction B_a.

D. Initial Field Current I_f

Fig.6 is the no-load characteristic of a typical generator, showing the relationship between the electromotive force of the no-load E_0 and the exciting current I_f. If one assumes that the magnetic fields under different operating condition are not saturated, it reads:

$$\frac{U_N}{I_{f0}} = const = \frac{E_0}{I_f} \tag{23}$$

i.e.,

$$I_f = E_0^* I_{f0} \tag{24}$$

From Fig.5, E_0^* is determined from

$$E_0^* = \sqrt{U^{*2} + I_a^{*2}R_a^{*2} + 2U^* I_a^* R_a^* \cos\varphi - I_{aq}^{*\,2} X_q^{*2}} + I_{ad}^* X_d^* \tag{25}$$

$$I_{ad}^* = I_a^* \sin(\Psi_0) \tag{26}$$

$$I_{aq}^* = I_a^* \cos(\Psi_0) \tag{27}$$

where R_a is the resistance of the armature coil.

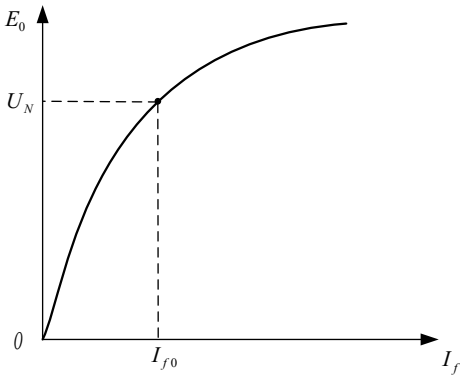

Fig. 6. The no-load characteristic curve of a generator.

E. Exact Field Current

The initial filed current I_f is determined from the assumption that the no-load characteristic curve is always in the linear segment in different operating conditions. However, the iron core will work in saturated conditions and the open circuit curve will work in the non-linear segments as long as the flux density is large enough. Therefore, the exact field current I_f is determined by repeatedly adjusting I_f in the FEM analysis of the rated and leading phase until the fundamental amplitude of magnetic field in the air gap is identical to that of the no-load condition in this paper

IV. Numerical Applications

To show the feasibility and accuracy of the proposed model and solution methodology, the coupled eddy current and temperature field as well as the losses of a 250MW hydro-generator in different operating conditions are computed. In order to compare the performances of different solution methodologies of section III, the field and armature currents are determined from two different methodologies: the traditional one using an analytical solution methodology (Methodology-I) and the proposed numerically based repeating methodology (Methodology-II). Fig. 7 and Fig. 8 depict, respectively, the air gap flux densities of the prototype generator under a 0.95 leading phase operation using methodologies I and II while Fig. 9 and Fig. 10 give the corresponding temperature field distributions in the press plate and finger. Fig. 11 and Fig. 12 present the iron losses distribution for two typical stator core laminations.

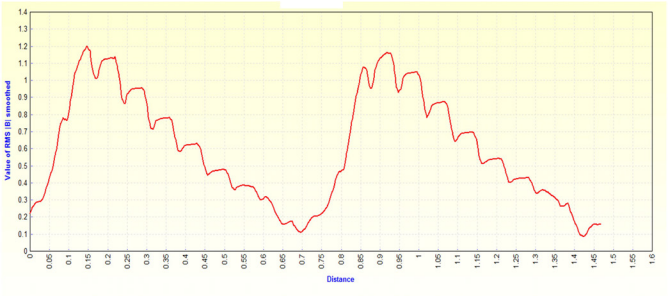

Fig.7. The air gap flux density under 0.95 leading phase (Methodology-I).

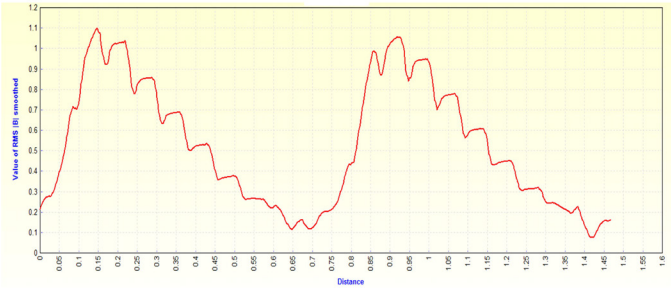

Fig.8. The air gap flux density under 0.95 leading phase (Methodology-II).

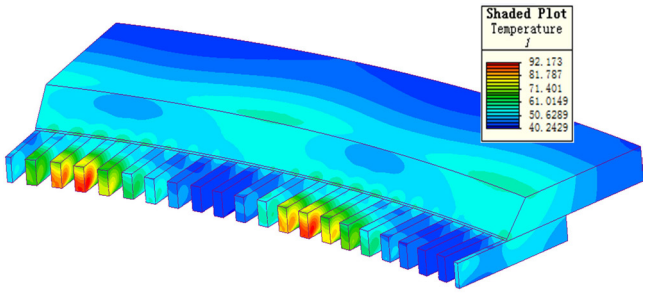

Fig.9. The temperature distribution in pressure finger and plate under 0.95 leading phase (Methodology-I).

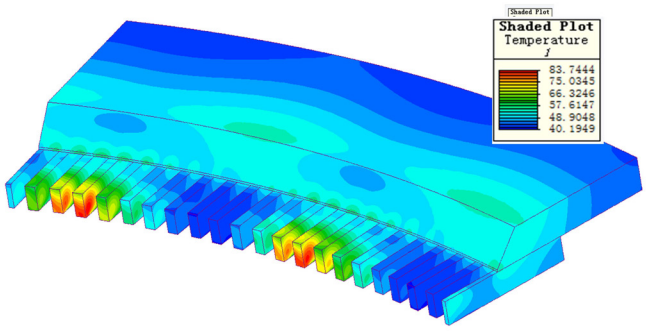

Fig.10. The temperature distribution in pressure finger and pressure plate under 0.95 leading phase (Methodology-II).

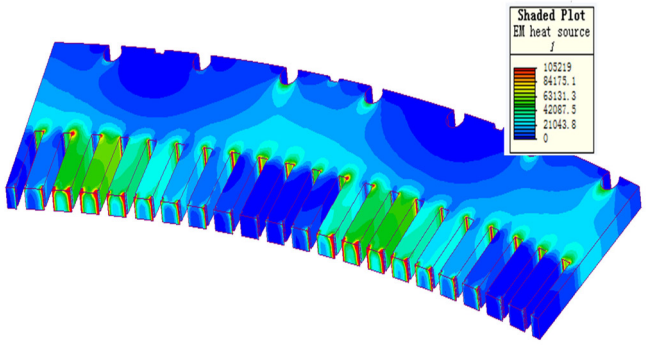

Fig.11. The iron losses distribution in stator core laminations without contact with pressure finger under 0.8 leading phase (Methodology-I).

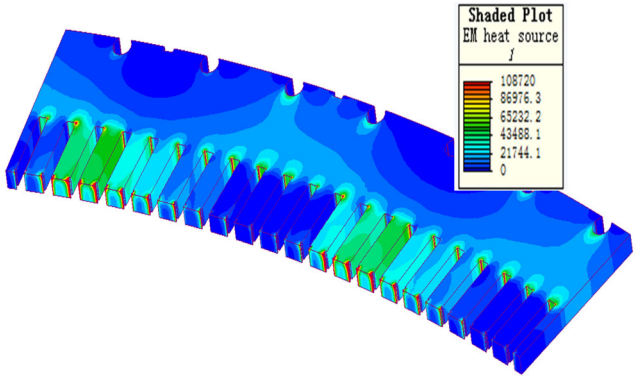

Fig.12. The iron losses distribution in stator core laminations without contact with pressure finger under 0.8 leading phase (Methodology-II).

From these numerical results, it can be seen that although there is a deviation in the absolute values of the fields, the distribution of the eddy current field and losses under different leading phase conditions is almost the same. It should be emphasized that the air gap flux density distribution determined using the proposed solution methodology is more close to the exact one in terms of both magnitude and distribution of the flux density.

Moreover, to give an intuitive image on the total losses obtained using the aforementioned two solution methodologies, Fig. 13 and Fig. 14 give the total losses of some typical structures. In these figures, core laminate 1 refers to the stator iron core laminate next to the pressure finger, and iron core lamination 2 refers to the residual stator iron core lamination. The amplitudes of the fundamental component of the flux densities in the air gap in the rated, 0.95 leading phase, and 0.8 leading phase operating conditions computed using the solution methodology I, are, respectively, 1, 0.88 and 0.88 (relative value); whiles those obtained using the proposed methodology II are 1, 1, and 1; evidencing further the high computational accuracy of the proposed solution methodology.

From these numerical results, it is reconfirmed that the generator's working state obtained using the proposed solution methodology is more consistent to the actual situation compared on that based on the traditional analytical methodology. More specially, the amplitude of the fundamental component of the flux density in the air gap under different operating conditions keeps unchanged for the proposed methodology.

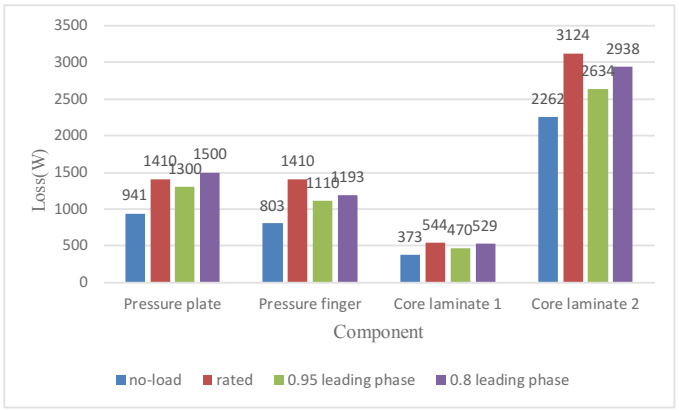

Fig. 13. The loss of typical structures using solution methodology I

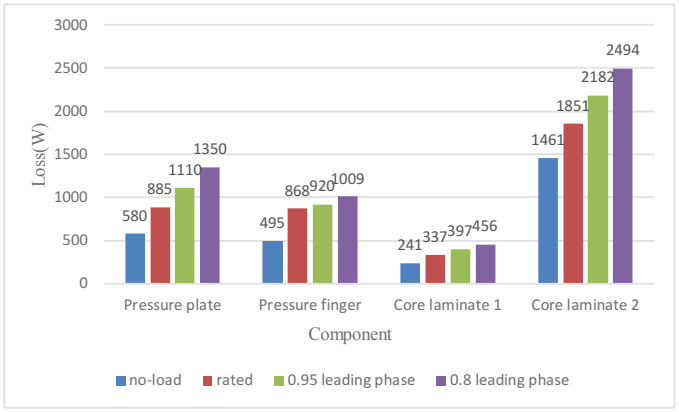

Fig. 14. The loss of typical structures using solution methodology II

V. Conclusions

The three dimensional models and methods for the coupled eddy current and temperature fields in the end regions of a large hydro-generator are proposed and implanted in this paper. The numerical results as reported have demonstrated that the proposed model and solution methodology will give more accurate computations as compared to the available approaches. According to the knowledge of the authors, there are relatively fewer literatures in recent years to report comprehensively the progress on this issue. The authors thus believe that this work would be helpful for engineers in computing the leading phase capacity of large hydro-generators.

References

[1] B. Frei-Spreiter, K. Reichert, "Calculation of end winding fields of turbo-generators by integral methods for modelling mechanical characteristics," *IEEE Transactions on Magnetics,* vol. 34, no.5, pp. 3636-3639.Sep, 1998.

[2] R. Albanese, F. Calvano, G. Dal Mut, F. Ferraioli, A. Formisano, F. Marignetti, R. Martone, A. Romano, G. Rubinacci, A. Tamburrino, and S. Ventre. "Coupled Three Dimensional Numerical Calculation of Forces and Stresses on the End Windings of Large Turbo Generators via Integral formulation," *IEEE Transactions on Magnetics,* vol. 48, no.2, pp. 875-878.Jan, 2012.

[3] Y. Y. Yao, H. X. Xia, G. Z. Ni, et al. "3-D eddy current analysis in the end region of a turbo-generator by using reduced magnetic vector potential," *IEEE Transactions on Magnetics,* vol. 42, no.4, pp. 1323-1326.Mar, 2006.

[4] Y. Hou, W. Li, F. Zhou, and S. Cheng, "Analysis and calculation of stator windings end part temperature field for large synchronous generator," *Proceedings of the Fifth International Conference on Electrical Machine*,

Shenyang, China, Aug. 1145-1148,2001.

[5] for end region of large turbogenerators," *Proceedings of the Eighth International Conference on Electrical Machines and Systems* (*ICEMS 2005*), Nanjing, China, Sep, 2079-2082, 2005.

[6] L. Yanping, H. Hao, and H. Gang, "Numerical calculation of end region electromagnetic field of large air-cooled turbogenerator,"*Automation Congress*, Hawaii, HI, USA, Dec, 1-5, 2008.

[7] L. K. Wang, F. Y. Huo, W. L. Li, et al. "Influence of Metal Screen Materials on 3-D Electromagnetic Field and Eddy Current Loss in the End Region of Turbogenerator, " *IEEE Transactions on Magnetics,* vol. 49, no.2, pp. 939-945.Feb, 2013.

[8] Y. P. Liang, P. Zhang, J. Chen, et al. "Eddy current losses of end structures for 1 000MW air-cooled hydro-generator", *Transactions of China Electrotechnical Society*, vol. 27, no.12, pp. 213-218.Dec, 2012.

[9] Y. P. Liang, H. R. Wang, J. T. Zhang, et al. "Research of end fields and eddy current losses for air-cooling steam-turbo-generator," *Electric Machines and Control*, vol. 14, no.1, pp. 29-34.Jan, 2010.

[10] H. X. Xia, Y. Y. Yao, S. M. Xiong, et al. "Magnetic-thermal coupling analysis end region of 1 000 MW turbine-generator", *Proceedings of the CSEE*, vol.28, no.14, pp. 118-122.May, 2008.

Ning Wang received the B.S. degree of electronic information science and technology from Northeast Electric Power University, Jilin, China, in 2011, and the M.S. degree of electrical engineering from Zhejiang University, Hangzhou, China, in 2014. She is currently pursuing Ph.D. degree of electrical engineering in Zhejiang University, Hangzhou, China. Her research mainly focuses on computational electromagnetics.

Huifang Wang received the B.Sc. and M.Sc. degrees from North China Electric Power University, Baoding, China, in 1995 and 1998, and the Ph.D. degree from Zhejiang University, Hangzhou, China, in 2006. Currently, she is an associate professor in the Electrical Engineering College of Zhejiang University, China. Her areas of interests are power system protection, condition based maintenance.

Shiyou Yang received the M.S. and Ph.D. degrees of electrical engineering from Shenyang University of Technology, Liaoning, China, in 1990 and 1995, respectively. He is currently a Professor in the Electrical Engineering College of Zhejiang University, China. His research mainly focuses on computational electromagnetics.